Combined One-Way and Two-Way Shape Memory in a Glass-Forming Nematic Network

Haihu Qin[†,⊥] **and Patrick T. Mather***[,†,‡,§]

Department of Macromolecular Science and Engineering, Case Western Reserve University, 2100 Adelbert Road, Cleveland, Ohio 44106, and Syracuse Biomaterials Institute and Department of Biomedical and Chemical Engineering, Syracuse University, Syracuse, New York 13244

Received October 12, 2008; Revised Manuscript Received November 17, 2008

ABSTRACT: Past research in the field of shape memory polymers has led to significant advancements in the areas of so-called one-way and two-way (reversible) shape memory. While one-way shape memory polymers allow indefinite fixing of a temporary shape until triggered thermally to recover to an equilibrium shape, two-way shape memory polymers feature muscle-like contraction on heating and expansion on cooling under tensile load, the latter anomalous elongation occurring due to an ordering transition. Previously, reversible actuation has been reported for liquid crystalline elastomers featuring a monodomain (uniformly aligned) structure, suggesting that such alignment is required for actuation. In this work, we have prepared a glass-forming polydomain nematic network that combines reversible actuation associated with a polydomain−monodomain transition with lower temperature one-way shape memory centered at T_g. To test separability of these phenomena, distinct deformations were achieved and temporarily fixed by (1) cooling through the isotropic−nematic transition under tensile load, (2) further bending the sample isothermally above T_g, and (3) cooling below T_g. Subsequent heating led to complete and sequential recovery of the same deformations in reverse order. Applications in multistage deployment of structures are envisioned.

Introduction

Shape memory polymers (SMPs) are an exciting class of materials receiving increasing attention during the past two decades due to their utility as soft actuators, and diverse reviews have appeared that examine this field from various perspectives.[1−7] Currently, two distinct, but equally important, types of shape memory materials are most widely studied. The first kind of SMP, termed "one way", features a chemically or physically cross-linked structure that is capable of "memorizing" its permanent shape and a "fixing/triggering temperature", T_{crit}, which could be the glass transition or melting point. (The interested reader is referred to one of the review articles, which details many examples of both SMP types.[2]) At temperatures higher than T_{crit}, the constituent network chains gain enough mobility to allow significant and reversible deformation upon application of stress. If such a deformed sample is then cooled to a temperature below T_{crit}, the same network chains become highly constrained, resulting in a fixing of the deformation such that it remains even after stress release. At this point, the material exists in a dormant, metastable state. When the material is reheated back to a temperature exceeding T_{crit}, the constituent polymer chains regain their mobility and the sample recovers to the original shape, driven by entropic elasticity.[8,9]

In the one-way shape memory effect, only the recovery step (e.g., length contraction) is spontaneous, while the deformation step (e.g., elongation) requires external intervention involving force application that overcomes entropic elasticity. Before deformation, each network chain exists in an entropy-maximizing configuration consisting of spherical Gaussian coils conformations. In response to deformation, the same network chains elongate, decreasing conformational entropy and increasing elastic free energy. As a result, some resistance to deformation is apparent, adding in total to the material's elastic modulus, E, following the form $E \sim 3NkT$, where N is the number density of nework chains (cross-link density), k is Boltzmann's constant, and T is the absolute temperature.[9] Quite recently, Bellin and co-workers[10,11] have prepared copolymer networks with two distinct *one-way* shape memory fixing mechanisms (either glass transition and crystallization or both crystallization-based) built into the same material. Interesting "triple shape" phenomena were reported.

A second type of shape memory phenomenon for polymers exists, termed "two-way shape memory", wherein mechanical activity occurs during both heating and cooling. Most reported two-way shape memory polymers are nematic liquid crystalline elastomers, although we have recently reported on a two-way shape memory effect in a cross-linked semicrystalline polymer.[12] Unlike conventional elastomers, nematic liquid crystalline elastomers (NLCEs) are capable of chain conformation changes apparently without the need of any external stress.[13] The polymer coil in the nematic state thermodynamically favors a prolate or oblate ellipsoidal conformation (depending on the macromolecular architecture) over a spherical conformation. As it is presently understood, heating an NCLE through the nematic−isotropic (NI) transition causes the constituent prolate network chains characteristic of the nematic state to contract to the spherical configuration of the isotropic phase. Collectively, a large macroscopic contraction in excess of 100%[14−16] is realized, and this contraction is reversed upon cooling back into the nematic phase. While this phenomenon is commonly referred to as "reversible contraction/extension", in the context of shape memory we prefer the term "two-way shape memory" to indicate that activity occurs both on heating and cooling without user intervention and in line with terminology of shape memory alloys (SMAs).[12,16,17] Two-way shape memory in a polydomain NLCE is possible but requires application of a finite (∼50 kPa) stress, as we will describe in this paper. We note that not all LCEs feature two-way shape memory response; indeed, one report has revealed one-way shape memory behavior in a smectic-C LCE featuring mesogen glass formation.[18]

* To whom correspondence should be addressed.
† Case Western Reserve University.
‡ Syracuse Biomaterials Institute, Syracuse University.
§ Department of Biomedical and Chemical Engineering, Syracuse University.
⊥ Current address: The Lubrizol Corporation, 29400 Lakeland Blvd, Wickliffe, OH 44092.

10.1021/ma8022926 CCC: $40.75 © 2009 American Chemical Society
Published on Web 12/08/2008

Scheme 1. Preparation Strategy of the Glass-Forming Nematic Network (P5tB-LCN)[a]

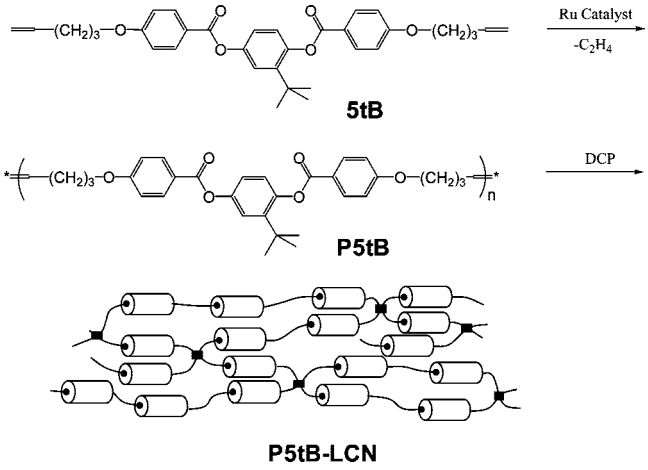

[a] P5tB is first prepared by ADMET polymerization, and then this unsaturated polymer is cross-linked by dicumyl peroxide (DCP) cure.

Here, we report on our observations of both one-way and two-way shape memory effects in a single cross-linked composition that exhibits a polydomain and glass-forming nematic phase, allowing very unique shape fixing and recovery phenomena. Characterization of the phase behavior and microstructure exhibited by the material revealed the underlying mechanisms responsible for shape memory behavior.

Experimental Section

Materials. A newly synthesized liquid crystalline diene, 2-*tert*-butyl-1,4-bis[4-(4-pentenyloxy)benzoyl]hydroquinone (5tB) was polymerized to an unsaturated liquid crystalline polyester (P5tB)[19] using acyclic diene metathesis (ADMET) polymerization and subsequently cross-linked with dicumyl peroxide (DCP) at 150 °C to yield P5tB-LCN. In contrast to NLCEs, a glass-forming nematic network (noncrystalline and T_g > room temperature) was obtained. This two-step preparation strategy of P5tB-LCN is shown in Scheme 1.

5tB Synthesis. While a detailed description on the synthesis and characterization (NMR, DSC, and polarized optical microscopy) of 5tB was published in our previous paper,[20] we would like to briefly restate the synthesis of 5tB here for reader convenience. 5tB was synthesized by esterification reaction between 5-penetenyloxybenzoic acid and *tert*-butylhydroquinone in the presence of 1,3-dicyclohexylcarbodiimide. The 5-pentenyloxybenzoic acid was prepared by reaction between 4-hydroxybenzoic acid and 5-bromo-1-pentene and then purified by recrystallization from ethanol. All reagents involved were reagent grade and used as purchased. The only exception is the *tert*-butylhydroquinone, which was recrystallized from toluene multiple times (usually three times) until colorless crystals were obtained. After synthesis, 5tB was purified by column chromatography with a mixed solvent of hexanes and ethyl acetate (volume ratio: 7:1) as the eluent. After the column chromatography treatment, some of the product was found to have crystallized out from the solvent. Nevertheless, the product was collected by evaporating almost all the solvent and then filtering to collect the solid compound. ^{1}H NMR in d_6-acetone gave δ: 8.16 (4H, m), 7.33 (1H, s), 7.22 (2H, t), 7.14 (4H, m), 5.95 (2H, m), 5.04 (4H, m), 4.16 (4H, t), 2.28 (4H, m), 1.93 (4H, m), 1.39 ppm (9H, s). DSC studies revealed that 5tB is a slowly crystallizing substance with the phase sequence on heating of crystal (80.6 °C) nematic (91.4 °C) isotropic.

P5tB Synthesis. P5tB was prepared and purified on a relatively large scale. The procedure was similar to the one described in our prior report.[19] Monomer, benzylidene−bis(tricyclohexylphosphine)-dichlororuthenium (first-generation Grubbs catalyst), and solvent (anhydrous toluene) amounting to 7.5 g, 0.22 g, and 18 mL, respectively, were charged into a dry and oxygen-free glass reactor. The polymerization system was stirred for 6 h at 55 °C under a continuous flow of nitrogen. The resulting polymer solution was diluted and later precipitated in methanol. After drying under vacuum at 50 °C, the crude polymer was dissolved in chloroform and purified with tri(hydroxymethyl)phosphine, though without first cleaving by vinyl ethyl ether (see ref 19). Accordingly, 5.0 mL of THP solution (22 vol % in 2-propanol) was added, and the mixture was stirred at 55 °C for 24 h. A thin layer of dark-brown liquid formed on the surface of the chloroform solution, which we understood to be the 2-propanol solution of the hydrophilic ruthenium species generated by the reaction between catalyst residual and THP. Without further separation, the mixture of both layers was then precipitated in a cosolvent of methanol and water (volume ratio: 90:10) to obtain a pure white polymer. The yield after all the purification steps was 6.0 g (~80%). Gel permeation chromatography (GPC) showed the number-average molecular weight to be 7.9 kDa with a polydispersity of 1.4, relative to polystyrene standards, while differential scanning calorimetry (DSC) and polarizing optical microscopy (POM) characterizations revealed the T_g and T_{NI} to be 64.8 and 177.4 °C, respectively. ^{1}H NMR in $CDCl_3$ gave δ: 1.38 (*tert*-butyl, 9H), 1.90 (aliphatic, 4H), 2,22 and 2.26 (aliphatic coupled with trans and cis C═C double bond, 4H), 4.06 (CH_2 next to the oxygen, 4H), 5.53 and 5.49 (trans and cis internal C═C double bonds, 2H), 5.05 and 5.86 (terminal double C═C bonds, trace), 6.98 (aromatic, 4H), 7.12 (aromatic, 2H), 7.23 (aromatic,1H), 8.16 (aromatic, 4H). The trans/cis ratio was determined to be about 68/32, and no isomerized structure was detected by ^{1}H NMR. A detailed NMR study, including the characterization of configuration of the double bond and isomerized structure by ^{1}H NMR, ^{13}C NMR, ^{1}H−^{1}H 2D NMR (COSY), and ^{1}H−^{13}C 2D NMR (HMQC), appears in our previous report.[19]

P5tB-LCN Synthesis. Cross-linkable blends of P5tB and dicumyl peroxide (DCP) were prepared by solvent casting from THF. As a typical example, a solution containing 0.9 g of P5tB and 0.1 g of DCP in 10 mL of THF was prepared to yield a homogeneous and clear solution at room temperature under stirring. The solution was then cast at room temperature for 24 h, evaporating the most of the solvent. Residual solvent was further removed by exposure to vacuum at room temperature for another 24 h. After drying, a white and brittle film was obtained. The cross-linkable blend containing 10 wt % DCP was then heated to 150 °C for 20 min to allow the sample to flow and fill a silicone mold. The sample was then further degassed for 20 min under vacuum at the same temperature to remove any trapped solvents. After that, the precursor, together with the mold, was moved to an autoclave which was preheated to 150 °C, and high-pressure nitrogen (0.69 MPa) was charged. The blend was cured under such a pressure and temperature for 24 h to obtain a turbid white, void-free sample. The gel fraction was determined to be 85% after extraction with THF for 24 h. However, in the present work, the sample was studied as synthesized without any extraction step.

Thermal and Viscoelastic Analyses. Phase behavior was analyzed using differential scanning calorimetry (DSC) on a TA Instruments DSC 2910 unit with a nitrogen purge, heating and cooling rates of 10 °C/min, and initial thermal history erasure by heating to 220 °c and back to room temperature. Linear viscoelastic thermo-mechanical properties of the materials were determined using dynamic mechanical analysis (DMA). A TA Instruments DMA 2980 apparatus was employed in tensile mode with a preload force of 10 mN, static stress/dynamic stress amplitude ratio ("force tracking") of 108%, a heating rate of 3 min °C/min, and an oscillation frequency of 1 Hz. We would like to note that the DMA test was challenging because the modulus of the material decreased more than 7000-fold after the glass transition (from 3 GPa at −100 °C to below 0.41 MPa at 151.5 °C, as illustrated in Figure 1b). Thus, a strain amplitude producing 9 N of force amplitude, which is the maximum of the instrument, will only generate a 1.3 mN force amplitude beyond T_g, which is too small to give a reasonable

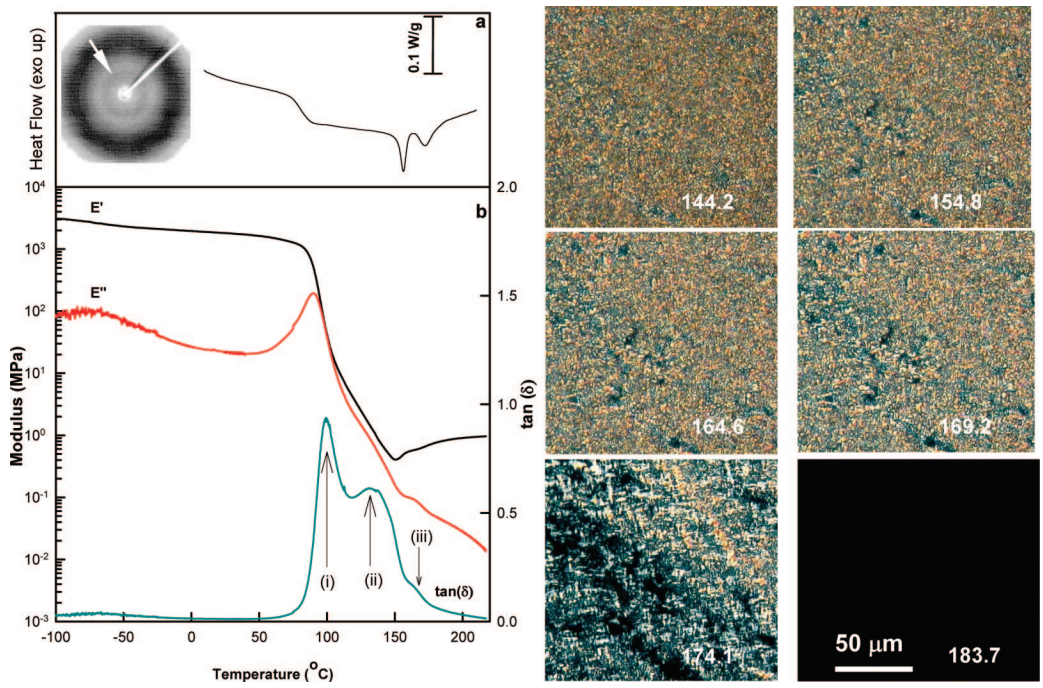

Figure 1. Characterization of P5tB-LCN cross-linked by 10 wt % DCP. (a) Second-heating DSC revealing one T_g at ca. 80 °C and two nematic−isotropic transitions centered at 156.3 and 172.5 °C. (inset) Wide-angle X-ray scattering pattern of an unstretched sample at room temperature, indicated a nematic glass. (b) DMA: Tensile storage modulus (black), loss modulus (red), and tan δ (green). Besides the damping peak at 100 °C due to the glass transition, there is a second damping peak at about 135 °C attributed to dynamic soft elasticity. The valley temperature between the two tan (δ) peaks is 118.5 °C, which later served as the boundary temperature between deformation I and II in our tandem shape memory experiments. (right) Hot-stage POM micrographs of the P5tB-LCN during heating at the rate of 5 °C/min to 220 °C. A tight, fine texture attributed to cross-linking was found at low temperatures, $T < 144.2$ °C. Heating from 144.2 to 183.7 °C led to birefringence disappearance, indicating a transition to isotropic phase.

signal/noise ratio. To overcome this issue, we adjusted the amplitude during the experiment, using a starting amplitude of 5 μm (0.035% strain) and adjusted to 125 μm (0.89% strain). As a result, the force amplitude was maintained slightly above 0.01 N and a good signal/noise ratio was achieved. The original sample size was 14.12 mm × 1.6 mm × 1.38 mm, and the maximum static displacement during the test was 1000 μm, which corresponded to a strain of 7%.

Microstructural Analyses. *Polarizing Optical Microscopy.* Liquid crystalline textures and thermal transitions of the TLCPs were investigated using hot-stage polarizing optical microscopy (POM). Samples were cross-linked directly between a glass slide and coverslip using the same conditions as described above for sample bars, but without applied pressure. After cooling to room temperature, the samples were then heated to 220 at 5 °C/min, removing thermal history, and then cooled to 30 at 5 °C/min. A second heating to 220 °C was conducted at 5 °C/min for micrograph collection. POM was conducted using an Olympus BX50 microscope equipped with a CCD camera (Panasonic GP-KR222) and a temperature-controlled hot stage (Instec STC 200). The samples were observed between crossed polarizers, allowing imaging of nematic-phase birefringence.

Wide-Angle X-ray Scattering. A Bruker GADDS-4 unit with a chromium source ($\lambda = 2.291$ Å) was used to determine the sample microstructure at molecular dimensions. The scattering patterns were collected on a HiStar area detector placed at a distance of 6 cm from the sample and featuring an array of 512 × 512 detection elements. The sample-to-detector distance allowed for diffraction data to be measured between $2.4° < 2\theta < 40°$, that is, $54.70 > d > 3.35$ Å, where d is the spacing of diffraction planes or scattering units. The X-ray power source was operated at 40 mA and 40 kV. The data were gathered and analyzed via a General Area Detector Diffraction System (GADDS) software version 3.317.

Shape Memory Testing. Several types of shape memory characterization experiments were conducted, including both qualitative and quantitative observations. Quantitative shape memory analyses employed a TA Instruments DMA 2980 apparatus operated in controlled ("static") force mode with prescribed variation in temperature and applied load and observation of the responding sample strain, as described for each experiment in the following.

"Two-Way" Shape Memory Characterization. The two-way shape memory effect of the P5tB-LCN under different stresses was characterized multiple times using the following procedure: Initially, at the high temperature of 162 °C, a prescribed stress was applied and the sample was annealed for 30 min to ensure thermal equilibration. Then the sample was cooled down slowly to 110 °C at the rate of 1 °C/min, during which period the sample was found to substantially elongate. After the temperature reached 110 °C, the sample was annealed for another 30 min to eliminate any possible temperature gradients. Finally, the sample was ramped back to 162 at 1 °C/min, with clear contraction occurring near T_{NI}, and annealed there for 30 min to recover any residual deformation. This protocol was repeated several times with different loads while recording sample length (and tensile strain) as a function of load (tensile strain) and temperature.

Two-Stage Shape Memory Characterization. Here, two procedures were followed: one for qualitative observations and the other for quantitative observations. (1) *Qualitative*. A sample was first heated on a heating plate to 200 °C, removed from the hot surface with a pair of tweezers, stretched, and cooled to room temperature. The stretched sample was then placed on another heating plate set to 100 °C, bent, and then cooled to room temperature. Sequential recovery of the two deformations was observed by placement of the stretched and bent sample first on the 100 °C heating plate and then on the 200 °C heating plate. The entire procedure was recorded as a digital movie using a CCD camera. (2) *Quantitative.* The two-stage shape memory effect was studied quantitatively with the following protocol. A sample was first annealed at 160 °C with a preload of 6.4 kPa (sample cross-sectional area was 1.56 mm^2) and then deformed by ramping the temperature to 118.5 at 1 °C /min. After annealing at 118.5 °C for 30 min, a secondary strain was introduced by increasing the stress at a rate of 12.8 kPa/min to a prescribed target value. Then, the sample was quenched to 40 °C and annealed for 10 min to eliminate

any temperature gradients. Subsequently, the load was removed at the same rate. For every stage of this protocol, the stress was prescribed and the strain was measured. Both the strains induced by (i) cooling below T_{NI} and (ii) force ramping were recovered during heating cycle to 160 at 1 °C /min, albeit over different ranges of temperature.

Nonmonotonic Strain Response Testing. Nonmonotonic strain response testing was also performed on TA DMA 2980 with controlled tensile force mode. A sample of 2.19 mm wide, 1.19 mm thick, and 5.34 mm long was used. The sample was loaded at room temperature to a controlled tensile stress of 20 kPa, following which the samples was heated from 40 to 180 °C at 1 °C/min while monitoring the tensile strain.

Results and Discussion

We begin with a description of the phase behavior that underpins the shape memory phenomena. As synthesized, P5tB-LCN is a polydomain nematic material with two adjacent nematic−isotropic transitions (T_{NI}), as indicated by differential scanning calorimetry (DSC), wide-angle X-ray diffraction (WAXD), and hot-stage polarized optical microscopy (POM). The DSC results (Figure 1a) show that P5tB-LCN has a T_g of 80 °C and two first-order transitions at centered at 156 and 173 °C, evidenced by two endothermic peaks. We suggest that the two transitions are both nematic−isotropic (NI) transitions based on the WAXD and POM data as included as the inset of Figure 1a and Figure 1c. In the diffraction pattern of the original P5tB-LCN in Figure 1a, essentially only a broad halo is present centered at the 2θ angle of 26.0°, which corresponds to the intermolecular spacing between the rodlike liquid crystalline mesogens. According to the Bragg equation, the *d*-spacing is calculated to be 5.1 Å. A weak and diffuse lower angle reflection (indicated with an arrow) is visible as well; this is common for nematics and not suggestive of smecticity. The absence of a diffraction pattern characteristic of any crystalline or smectic phase rules out the existence of melting, smectic−nematic, or smectic−isotropic transitions. In addition, POM results (Figure 1c) show the transition from a birefringent phase to an isotropic phase over the broad temperature range from 144.2 to 183.7 °C, which is the same temperature range of the two endothermic peaks observed in DSC results (Figure 1a).

Taken with our DSC and WAXS observations, the only plausible explanation is that P5tB-LCN is a nematic network that becomes isotropic through the two nematic−isotropic (NI) transitions. In POM micrographs, we do observe a few black spots that start to form at 154.8 °C, and those black spots do not significantly expand for next 15 °C. These observations suggest two separate nematic phases with different T_{NI} transitions. Indeed, from 154 to 169 °C, the transition during this 15 °C span seems far less significant than the transition that occurs between 169 and 174 °C, in agreement with the bimodal DSC result. The biggest black spot is about 5 μm in size, indicating phase separation at that scale. Furthermore, the material is apparently polydomain in nature, identified by both nonoriented WAXD diffraction pattern (Figure 1a) as well as the very fine nematic textures in POM with heterogeneity on the scale of 5 μm (Figure 1c). We note that we did not observe the typical Schlieren textures that are common in low molecular weight (thus low viscosity) liquid crystals. Instead, we observed a very fine texture without resolution of disclination lines, as is commonly reported for thermotropic polymers.[21]

We surmise that the origin of a bimodal N−I transition in our P5tB-LCN system lies in the detailed phase behavior during cross-linking. According to a study by Warner,[22] any fraction of LCE cross-linked in the nematic phase is anticipated to have higher T_{NI} than the fraction of sample cross-linked in isotropic phase. Indeed, we observed under hot-stage POM that the cross-linking mixture (P5tB and 10 wt % DCP) was in a biphase state at the cross-linking temperature of 150 °C, as DCP slightly lowered the range of clearing temperatures—intrinsically broad—to span the curing temperature (lower curing temperatures are not effective with the chosen peroxide). In addition, we compared cross-linking at 160 and 150 °C, revealing that samples cured at 160 °C resulted in a larger endotherm for the first (lower temperature) transition than for the second (higher temperature) transition. Thus, cross-linking at 160 °C occurs with a greater portion of the sample in the isotropic state—this portion having a lower clearing point—further supporting our explanation. Despite this complication, the existence of two NI transitions is not essential to our findings, as we explain below.

P5tB-LCN exhibits dynamic mechanical properties typical (though quite unique) of a nematic network.[23] Of particular interest is a very strong and broad peak in the loss tangent trace between the T_g and T_{NI}. This intermediate peak is taken to be a manifestation of "dynamic soft elasticity", described below. Figure 1b shows the DMA data together with the DSC (Figure 1a) of the P5tB-LCN. At temperatures below 70 °C, the sample is glassy with the storage modulus (black) as high as 2 GPa. A small mechanical relaxation is observed, centered at −70 °C, which we attribute to the onset (on heating) of local molecular motions involving either the flexible spacer or the *tert*-butyl groups. As the temperature reaches 80 °C, the storage modulus starts to dramatically decrease because of the glass transition. This transition is also manifested in the peaks of both the loss modulus (red) and tan δ (cyan) traces at 80.2 and 99.6 °C (arrow i), respectively. Beyond the glass transition, the tan δ curve shows a second major peak at 135 °C, which is similar in intensity (greater than 0.5) and broader than the glass transition peak. This transition is attributed to a nematic-based mechanical relaxation. We postulate that at this condition of stress and temperature the nonaligned nematic ellipsoidal coils undergo cyclic reorientation (with stress overcoming Frank elasticity of domains[24]) toward the loading direction, dissipating energy. If a quasi-static stress of the same magnitude as the peak stress (i.e., exceeding a threshold stress) were applied, the same nematic domains would stretch and align, resulting in extensive deformation and a monodomain-like structure. While this phenomenon may be termed soft elasticity, the transition corresponding to the peak in tan δ curve is referred to as the polydomain−monodomain "transition" (T_{PM}) and the phenomenon itself "dynamic soft elasticity" after Clarke and coworkers.[23] We note that the PM "transition" is not a first-order thermodynamic transition in the usual sense, as there is no phase change involved. Finally, as the temperature approaches T_{NI}, tan δ decreases due to the disappearance of the nematic phase and thus this particular mechanical relaxation.

Compared with glass and polydomain−monodomain transitions, the nematic−isotropic transition is far less prominent in DMA. Nevertheless, the storage modulus shows two clear increases with temperature while the loss modulus exhibits two tiny negative peaks through the two N−I transitions. As a result, the tan δ curve exhibits two "dips" (not peaks) during both T_{NI} transitions at 156 and 173 °C. Beyond that, the storage modulus stabilizes at a plateau value of 1 MPa while tan δ nearly vanishes.

We found that P5tB-LCN exhibits a good two-way shape memory effect despite its polydomain nature. Figure 2 shows the two-way shape memory cycles under different preload tensile stresses (the engineering stresses were 3.7, 7.3, 11.0, 18.4, 25.7, and 36.7 kPa from trace i to vi, relative to the original cross-sectional area of 2.72 mm^2). Maintaining constant load, the sample elongates spontaneously during the course of cooling (the lower branch of the looplike curves) to 110 at 1 °C/min. The amplitude of this two-way actuation, which we calculate as the strain difference between 162 and 110 °C, is as high as

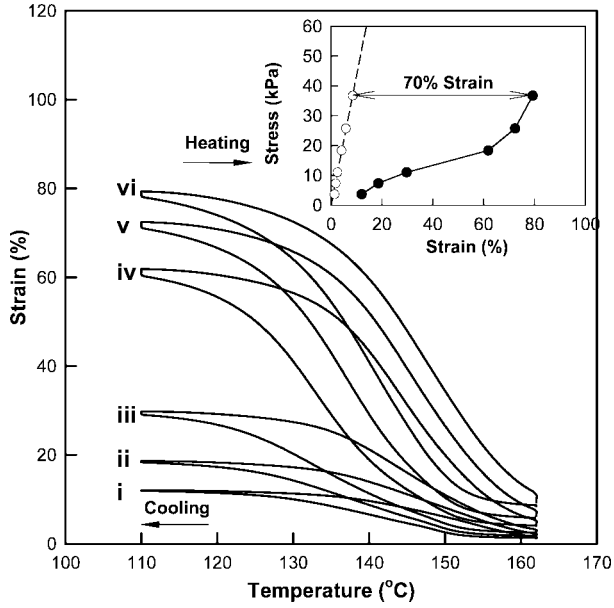

Figure 2. Two-way shape memory cycles of P5tB-LCN under stresses of (i) 3.67, (ii) 7.34, (iii) 11.01, (iv) 18.35, (v) 25.68, and (vi) 36.70 kPa. Inset: maximum strain at 110 °C (closed symbol) and original strain at 162 °C (open symbol) versus applied stress during the two-way shape memory cycle. A soft elasticity plateau is apparent at 110 °C. The amplitude of actuation is seen to be about 70%.

70% at a stress of 36.7 kPa. When heated back to 162 °C at the same rate, the samples gradually recover to their original length. Hysteresis (temperature breadth at half the actuation strain) in the response is evident and ranges from 5 to 12 °C, depending on the applied stress.

As introduced previously, the two-way shape memory effect usually requires monodomain liquid crystalline structures. However, during the synthesis of the P5tB-LCN, we did not utilize any method, such as surface rubbing, magnetic field, or mechanical stretch/shearing to align the material. Consequently, the P5tB-LCN obtained was a *polydomain* liquid crystalline material as discussed previously in the context of our WAXD and POM results of Figure 1. Instead, we postulate that the two-way shape memory effect we observe for P5tB-LCN follows a different mechanism.

We suggest a mechanism involving the concept of soft elasticity, discussed above. At the network chain level, as the temperature decreases through the isotropic−nematic transitions—but before elongation—the spherical network chains elongate to form an ellipsoidal shape, and their constituent mesogens align locally as a nematic phase. However, since the sample is not aligned, this chain-level elongation is macroscopically (>texture scale) "isotropic" and does not accumulate to a significant strain. However, when the temperature reaches conditions for the polydomain−monodomain transition, T_{PM} = 135 °C (Figure 1b), the applied stress exceeds a threshold stress (~12 kPa in this case, as we will discuss in next paragraph) and dramatic elongation occurs. This deformation process can be regarded essentially the same as the "soft elasticity", but achieved by changing temperature, not the stress or strain. To recover this strain, the sample is heated to above T_{NI}, and the ellipsoidal nematic coil shrink to the spherical shape of the isotropic phase, resulting in contraction. This recovery process is identical to the recovery/contract process observed in the monodomain nematic networks, despite distinct origins of the initially aligned state.

The inset of Figure 2 provides supporting evidence to the above mechanism by revealing the close relationship between two-way shape memory effect and soft elasticity. In the inset, we plot the maximum strain (the strain after cooled to 110 °C) versus stress (closed symbols). The plot clearly reveals a plateau characteristic of soft elasticity. The plateau of the curve obtained from the two-way shape memory cycles has a threshold stress of about 12 kPa and spans a strain range from 20 to 70%. In contrast, at temperatures above T_{NI}, the sample does not display soft elasticity. The plot of original strain (i.e., before spontaneous elongation on cooling) at 162 °C (open symbols) is nearly linear with the stress. By linear regression (dashed line), the modulus of the sample was measured to be 0.43 MPa at 162 °C, close to that determined by DMA experiments in Figure 1 (0.57 MPa). Note that the plot of strain at 110 °C versus the preload stress does not seem to pass through the origin. We surmise that it is because of the thermal expansion of the DMA fixture since we defined the zero position at 162 °C.

Our suggested mechanism is further consistent with the hysteresis observed between the deformation on cooling and recovery on heating in the two-way shape memory cycle as observed in Figure 2. Deformation occurs through the polydomain−monodomain transition, which occurs between the T_g and T_{NI} (135 °C as determined by DMA, but stress-dependent). On heating, the recovery happens at the nematic−isotropic transition. Indeed, researchers studying monodomain LCEs reported that the elongation strain of soft elasticity decreases linearly with the nematic order parameter and becomes zero at the T_{NI} temperature.[15] As discussed previously, P5tB-LCN actually has two NI transitions, which we surmise correspond to the portions of each sample cross-linked in the isotropic and nematic phases. However, we found that only the first (lower temperature) NI transition, which is attributed to the part of the sample cured in the isotropic phase, is found capable of "triggering" the two-way shape memory effect and soft elasticity. This surprising observation was also reported by Kuepfer,[15] who found that LCE samples cross-linked in the isotropic phase exhibited better soft elasticity, in the form of lower threshold stress, than those cross-linked in the nematic state.

Regarding actuation amplitude, the polydomain P5tB-LCN exhibits a quite large two-way shape memory effect that is comparable with monodomain LCEs. Considering the two-way shape memory mechanism discussed above, a threshold stress must be exceeded to generate significant deformation in polydomain LCNs, and there will be a hysteresis between deformation and recovery. For monodomain LCEs, there are no such theoretical limitations, although a finite applied stress is still a practical necessity of experiments to keep the samples straight for elongation measurements and, more importantly, to generate some work output during the actuation. For applications where hysteresis is not a critical issue, polydomain LCNs may offer a desirable, simplified alternative to their monodomain counterparts since they do not require alignment procedures during processing.

P5tB-LCN also features one-way shape memory triggered/fixed by its glass transition (T_g) at 80 °C. Deformations applied above T_g could be fixed by cooling below T_g and were recovered completely by reheating. Since the two shape memory effects have sharply distinct mechanisms and are separated by a wide temperature gap (>70 °C), the two types of deformation and recovery proved to function independently. In particular, separate deformations achieved by soft elasticity on cooling and by additional stress application (even in a different direction) between T_g and T_{NI} could be completely fixed in combined form below T_g and recovered in reverse order upon heating.

As an example, direct visualization of the two-stage shape memory effect is demonstrated in Figure 3, which clearly shows well resolved two-stage recovery. The original sample was a straight bar with dimensions of 1.5 mm × 1 mm × 20 mm (W × T × L). Before the experiment, the sample was first heated

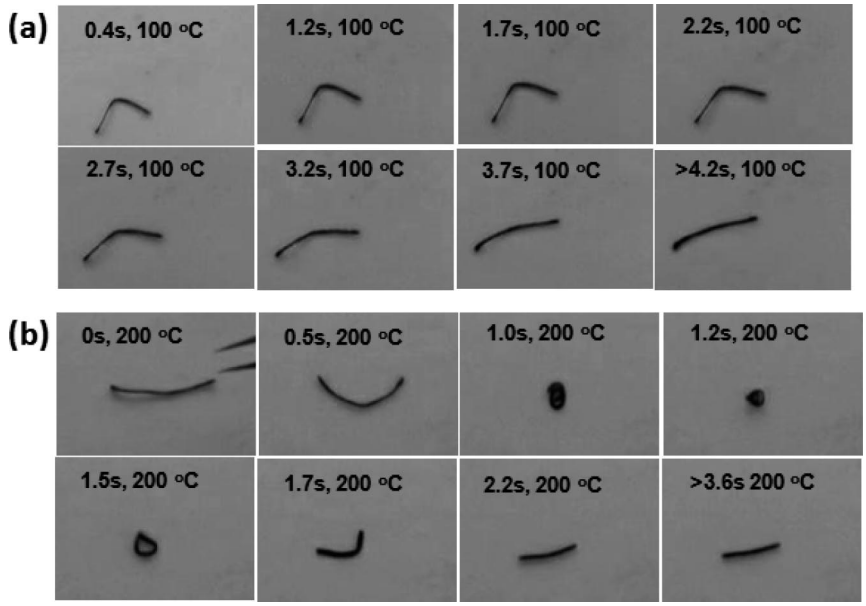

Figure 3. Sequential shape recovery of P5tB-LCN. Series (a): initial unbending recovery where the sample unbent itself at about 100 °C in about 3.7 s but did not shrink at this temperature. Series (b): second shrinking recovery where the sample shrank to its original length (22 mm) in about 2.2 s after the sample heated to 200 °C. Transient thermal gradients caused dramatic, though transient, coiling during shrinkage. All pictures feature the same magnification, and the equilibrium (and starting) sample length is 20 mm. The original video is shown in the Supporting Information.

to isotropic state by being placed on top of a heating plate maintained at 200 °C. The sample was next removed from the hot surface with a pair of tweezers and stretched. During the stretch step, the sample cooled from 200 °C to below T_g and all the deformations were fixed. Then, the deformed sample was placed on another hot plate preheated to 100 °C, above T_g but below T_{PM}. At this stage, the one-way shape memory fixing of any stress in excess of the stress plateau (Figure 2, inset) was recovered and observed as a slight contraction of the sample. While in contact with the heating plate at 100 °C, the sample was further *bent* and then cooled below T_g, allowing fixing of the combined first and second deformations. Heating of this sample led to separate and dramatic recovery of the intermediate and final (equilibrium) shapes. Series "a" of Figure 3 shows the first stage recovery of the sample. For this, the sample was place on the top of a hot stage preheated to about 100 °C, a temperature above T_g (80 °C) but significantly below T_{NI}. The sample rapidly unbent (within 4 s) but did not yet shrink. To trigger the second stage recovery (tensile shrinkage), the sample was next moved to another hot plate preheated to 200 °C (T_{NI} + 40 °C). At that temperature, the sample shrank to its original length in less than 2.2 s, as shown in series "b" of Figure 4. Because of heat transfer asymmetry intrinsic to hot-plate heating, the sample underwent significant coiling as one face (that contacting the plate) shrinks more than the other, temporarily. By the end of the transient event the sample is straight again, indicating completion of two-stage recovery. A digital video of the sequential recovery of this sample is available as Supporting Information.

Quantitative Characterization of Sequential Shape Memory Effects. Figure 4 shows sequential shape memory cycle performed on a DMA. The cycle starts at 160 °C with a low stress of 6.5 kPa (arrow). Cooling the sample to 118.5 at 1 °C/min led to elongation that was annealed isothermally for 30 min (red). This isostress deformation, symbolized as "deformation I" in Figure 4, follows the two-way shape memory mechanism. Next, a secondary strain was introduced isothermally by increasing the stress to a target value 64 kPa over 5 min. This secondary deformation, symbolized as "deformation II" (blue), is isothermal and graphically orthogonal to deformation I. Cooling to 40 °C allowed near-perfect fixing of both deformations as revealed by strain invariance while unloading (pink). Heating continuously to 160 °C (1 °C/min); both deformation I and deformation II were recovered in reverse order, the strain recovery rate (orange) clearly revealing the dual recovery behavior since two recovery peaks are present. We note that such a shape memory cycle gives us less resolved two stage recovery than shown in Figure 3, which we attribute to differences in protocol.

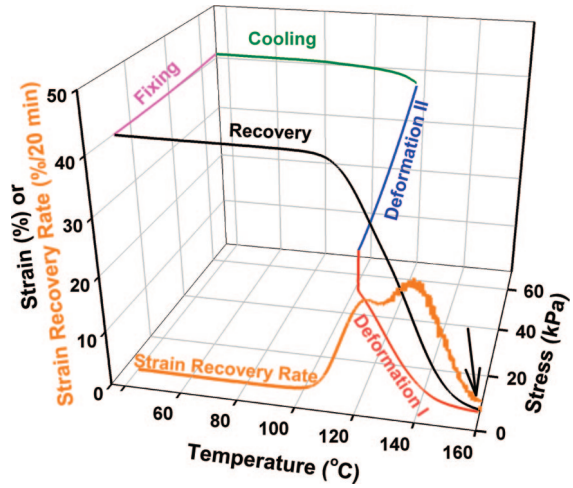

Figure 4. Tandem shape memory effect of P5tB-LCN. Beginning at 160 °C and 6.5 kPa (arrow), the sample elongated during cooling (1 °C/min) to 118.5 °C (red, deformation I). Further stretching occurred by application of a secondary stress of 58.5 kPa (blue, deformation II). After cooling to 40 °C, the secondary stress was unloaded (pink) and the sample was heated (1 °C/min) to 160 °C (black), revealing sequential recovery of the deformations in reverse order. The strain recovery rate (orange) shows a bimodal recovery.

The *first* stage recovery of recovery in Figure 4 is directly correlated with the *second* deformation, "deformation II". Figure 5 shows the strain recovery rate curves of the dual shape memory cycles with differing secondary stress increments (0, 6.5, 26.0, 58.5, and 91.0 kPa, from (i) to (v), respectively) while the initial stress was kept constant at 6.5 kPa. For better

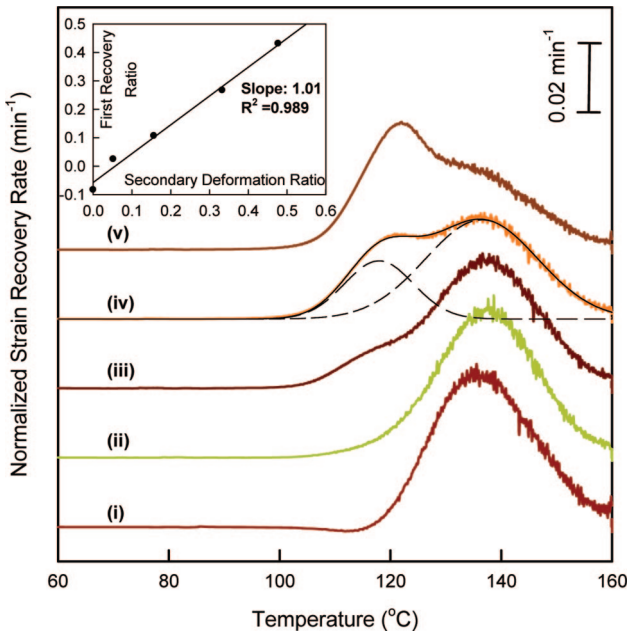

Figure 5. Normalized strain recovery rate curves of the tandem shape memory effect under different secondary deformation stresses of (i) 0, (ii) 6.5, (iii) 26.0, (iv) 58.5, and (v) 91.0 kPa. Each recovery rate curve can be resolved into two Gaussian peaks with high accuracy. In (iv) the two dashed lines are the two Gaussian peaks while the solid line is the sum, which overlaps with the raw data very well. Inset: linear correlation between the "secondary deformation ratio" (the ratio of deformation II over the total deformation) and the "first recovery ratio" (the area of the first recovery peak) from the strain recovery rate curve.

comparison, the curves are normalized so that the peak area is unity in each curve. The bimodal strain recovery persists in all cases, with clearly larger first recovery peaks for higher secondary stresses used in the tandem shape memory cycle.

Quantitative analysis of such a correlation was achieved by fitting the bimodal recovery rate curves with two Gaussian peaks (Peakfit). For explanatory purposes, the regression result of curve iv in Figure 5 is shown. The two dashed-line curves are the two Gaussian peaks of curve iv, while the overall regression curve (black solid) overlapped almost perfectly with the raw data. High correlation coefficients (>0.995) were found for all five of the strain recovery rate curves. By plotting the ratio of the first stage recovery rate to the total recovery rate versus the "secondary strain ratio" (defined as the ratio of deformation II to the sum of deformations I and II), a linear correlation is revealed (inset of Figure 5). The linear regression (solid line) produced a slope of 1.01 and a correlation coefficient of 0.989, indicating that first recovery is selectively derived from the secondary strain. Thus, the two mechanisms are independent.

Finally, as a second and distinct demonstration of unique shape memory response, we show in Figure 6 the consequence of loading P5tB-LCN in the glassy state and then continuously heating through T_g and T_{NI}. The stress applied, 20 kPa, is very small but in excess of the stress plateau required for soft elasticity, as shown in Figure 2. Surprisingly, a nonmonotonic temperature response was observed: in the nematic phase the sample elongates to a strain of 85%, peaked near $T = T_{PM}$, but then contracts to a strain of 3.5% during isotropization. Unloading the specimen removed all tensile strain completely, while cooling again under load (data not shown) caused elongation as in Figure 2 and renders the effect incapable of repeated cycling. This phenomenon is unprecedented to the best of our knowledge and is attributed to the combination of glass-forming and soft-elasticity attributes in the same composition.

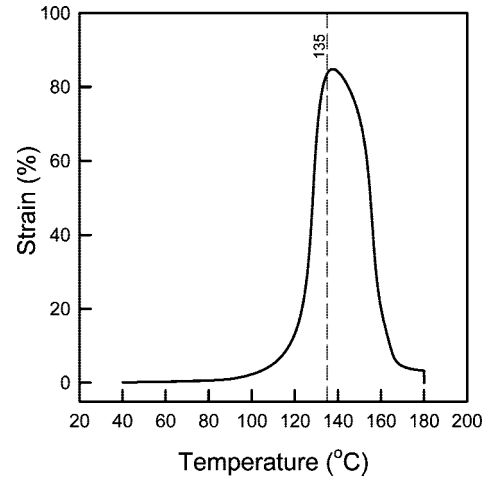

Figure 6. Nonmonotonic strain response when P5tB-LCN is heated under a tensile stress of 20 kPa at a rate of 1 °C/min through T_g (80 °C), T_{PM} (135 °C), and finally T_{NI} (complete at ca. 180 °C).

It may be useful for autonomous devices, such as a smart valve that opens for certain temperatures.

In summary, by cross-linking a thermotropic unsaturated polyester, a glass-forming, polydomain nematic network (P5tB-LCN) was obtained. This material exhibited both one-way and two-way shape memory effects related to the glass transition and polydomain soft elasticity intrinsic to the nematic phase, respectively. When used in tandem, two sequential and independent deformation can be applied and fixed. Subsequent continuous heating leads to recovery of shapes in the reverse order of fixing, indicating a novel two-stage shape memory effect. We envision a wide variety of deployment events possible through many permutations of the two temporary shapes. Further, we anticipate additional new phenomena to be possible through manipulation of the temperatures involved. For example, if the hysteresis in two-way shape memory (Figure 2) were made to overlap with T_g, then soft-elasticity-based elongation could be suspended by supercooling below T_g and later activated upon heating. Consequently, the surprising and entirely new nonmonotonic strain−temperature response of Figure 6 could be cycled indefinitely.

Acknowledgment. This research was supported by AFOSR/NL under Contract F4920-00-1-0100 and NSF under Grant DMR-0758631.

Supporting Information Available: Two AVI movies illustrating the tandem shape recoveries (unbend−shrink and untwist−shrink) of P5tB-LCN; description of the preparation of the monomers and polymers and more quantitative characterization of the tandem shape memory using DMA. This material is available free of charge via the Internet at http://pubs.acs.org.

References and Notes

(1) Lendlein, A.; Kelch, S. *Angew. Chem., Int. Ed.* **2002**, *41*, 2034–2057.
(2) Liu, C.; Qin, H.; Mather, P. T. *J. Mater. Chem.* **2007**, *17*, 1543–1558.
(3) Dietsch, B.; Tong, T. *J. Adv. Mater.* **2007**, *39*, 3–12.
(4) Gunes, I. S.; Jana, S. C. *J. Nanosci. Nanotechnol.* **2008**, *8*, 1616–1637.
(5) Mano, J. F. *Adv. Eng. Mater.* **2008**, *10*, 515–527.
(6) Ratna, D.; Karger-Kocsis, J. *J. Mater. Sci.* **2008**, *43*, 254–269.
(7) Rousseau, I. A. *Polym. Eng. Sci.* **2008**, in press.
(8) Rubinstein, M.; Colby, R. H. *Polymer Physics*; Oxford University Press: New York, 2003; p 454.
(9) Treloar, L. R. G. *The Physics of Rubber Elasticity*, 3rd ed.; Oxford University Press: Oxford, 1975; p 310.
(10) Bellin, I.; Kelch, S.; Langer, R.; Lendlein, A. *Proc. Natl. Acad. Sci. U.S.A.* **2006**, *103*, 18043–18047.

(11) Bellin, I.; Kelch, S.; Lendlein, A. *J. Mater. Chem.* **2007**, *17*, 2885–2891.
(12) Chung, T.; Romo-Uribe, A.; Mather, P. T. *Macromolecules* **2008**, *41*, 184–192.
(13) Warner, M.; Terentjev, E. M. *Liquid Crystalline Elastomers*; Oxford University Press: Oxford, 2003.
(14) Thomsen, D. L., III.; Keller, P.; Naciri, J.; Pink, R.; Jeon, H.; Shenoy, D.; Ratna, B. R. *Macromolecules* **2001**, *34*, 5868–5875.
(15) Kuepfer, J.; Finkelmann, H. *Macromol. Chem. Phys.* **1994**, *195*, 1353–1367.
(16) Kundler, I.; Finkelmann, H. *Macromol. Rapid Commun.* **1995**, *16*, 679–686.
(17) Terentjev, E. M. *J. Phys.: Condens. Matter* **1999**, *11*, R239−R257.
(18) Rousseau, I. A.; Mather, P. T. *J. Am. Chem. Soc.* **2003**, *125*, 15300–15301.
(19) Qin, H. H.; Chakulski, B. J.; Rousseau, I. A.; Chen, J. Z.; Xie, X. Q.; Mather, P. T.; Constable, G. S.; Coughlin, E. B. *Macromolecules* **2004**, *37*, 5239–5249.
(20) Rousseau, I. A.; Qin, H. H.; Mather, P. T. *Macromolecules* **2005**, *38*, 4103–4113.
(21) Larson, R. G. *The Structure and Rheology of Complex Fluids*; Oxford University Press: New York, 1998; Chapter 10; p 688.
(22) Warner, M.; Gelling, K. P.; Vilgis, T. A. *J. Chem. Phys.* **1988**, *88*, 4008–4013.
(23) Clarke, S. M.; Tajbakhsh, A. R.; Terentjev, E. M.; Remillat, C.; Tomlinson, G. R.; House, J. R. *J. Appl. Phys.* **2001**, *89*, 6530–6535.
(24) Mather, P. T.; Jeon, H. G.; Han, C. D.; Chang, S. *Macromolecules* **2000**, *33*, 7594–7608.

MA8022926